

# Small-angle neutron scattering reveals the effect of Mo on interphase nano-precipitation in Ti-Mo micro-alloyed steels

Wang, Yiqiang; Clark, Samuel James; Cai, Biao; Venero, Diego Alba; Yan, K; Gorley, Michael J; Surrey, Elizabeth; McCartney, David; Sridhar, Seetharaman S; Lee, Peter D

DOI:

[10.1016/j.scriptamat.2019.08.016](https://doi.org/10.1016/j.scriptamat.2019.08.016)

License:

Creative Commons: Attribution-NonCommercial-NoDerivs (CC BY-NC-ND)

*Document Version*

Peer reviewed version

*Citation for published version (Harvard):*

Wang, Y, Clark, SJ, Cai, B, Venero, DA, Yan, K, Gorley, MJ, Surrey, E, McCartney, D, Sridhar, SS & Lee, PD 2020, 'Small-angle neutron scattering reveals the effect of Mo on interphase nano-precipitation in Ti-Mo micro-alloyed steels', *Scripta Materialia*, vol. 174, pp. 24-28. <https://doi.org/10.1016/j.scriptamat.2019.08.016>

[Link to publication on Research at Birmingham portal](#)

## General rights

Unless a licence is specified above, all rights (including copyright and moral rights) in this document are retained by the authors and/or the copyright holders. The express permission of the copyright holder must be obtained for any use of this material other than for purposes permitted by law.

- Users may freely distribute the URL that is used to identify this publication.
- Users may download and/or print one copy of the publication from the University of Birmingham research portal for the purpose of private study or non-commercial research.
- User may use extracts from the document in line with the concept of 'fair dealing' under the Copyright, Designs and Patents Act 1988 (?)
- Users may not further distribute the material nor use it for the purposes of commercial gain.

Where a licence is displayed above, please note the terms and conditions of the licence govern your use of this document.

When citing, please reference the published version.

## Take down policy

While the University of Birmingham exercises care and attention in making items available there are rare occasions when an item has been uploaded in error or has been deemed to be commercially or otherwise sensitive.

If you believe that this is the case for this document, please contact [UBIRA@lists.bham.ac.uk](mailto:UBIRA@lists.bham.ac.uk) providing details and we will remove access to the work immediately and investigate.

1 **Small-angle neutron scattering reveals the effect of Mo on interphase nano-precipitation**  
2 **in Ti-Mo micro-alloyed steels**

3

4 Y. Q. Wang<sup>a\*, b</sup>, S. J. Clark<sup>b, c</sup>, B. Cai<sup>d</sup>, D. Alba Venero<sup>e</sup>, K. Yun<sup>f</sup>, M. Gorley<sup>a</sup>, E. Surrey<sup>a</sup>, D.  
5 G. McCartney<sup>b, g</sup>, S. Sridhar<sup>h</sup>, P. D. Lee<sup>b, c\*</sup>

6

7 <sup>a</sup> *United Kingdom Atomic Energy Authority, Culham Science Centre, Abingdon, OX14 3DB, UK*

8 <sup>b</sup> *Research Complex at Harwell, Rutherford Appleton Laboratory, Harwell, OX11 0FA, Oxfordshire, UK*

9 <sup>c</sup> *Department of Mechanical Engineering, University College London, Torrington Place, London WC1E 7JE,*  
10 *UK*

11 <sup>d</sup> *School of Metallurgy and Materials, University of Birmingham, Birmingham, UK*

12 <sup>e</sup> *ISIS, STFC Rutherford Appleton Laboratory, Didcot, Oxfordshire, OX11 0QX, UK*

13 <sup>f</sup> *School of Materials, University of Manchester, Manchester, M13 9PL, UK*

14 <sup>g</sup> *Advanced Materials Group, University of Nottingham, Nottingham, NG7 2RD, UK*

15 <sup>h</sup> *George S. Ansell Department of Metallurgical and Materials Engineering, Colorado School of Mines, Golden,*  
16 *CO 80401, USA*

17 \* Corresponding authors: Yiqiang Wang ([yiqiang.wang@ukaea.uk](mailto:yiqiang.wang@ukaea.uk)) and Peter Lee ([peter.lee@ucl.ac.uk](mailto:peter.lee@ucl.ac.uk))

18

19

20

21

22

1 **Abstract**

2 Ti-containing micro-alloyed steels are often alloyed with molybdenum (Mo) to reduce nano-  
3 precipitate coarsening, although the mechanism is still disputed. Using small angle neutron  
4 scattering we characterised the precipitate composition and coarsening of Ti-alloyed and Ti-  
5 Mo-alloyed steels. The results demonstrate ~25 at.% of Ti is substituted by Mo in the (Ti,  
6 Mo)C precipitates, increasing both the precipitate volume percent and average size. Mo  
7 alloying did not retard precipitation coarsening, but improved lattice misfit between  
8 precipitate and matrix, contributing to better aging resistance of the Ti-Mo-alloyed steel. This  
9 new understanding opens opportunities for designing aging-resistant micro-alloyed steels  
10 with lean alloying elements.

11

12

13

14

15

16

17

18

19 **Keywords:** Micro-alloyed steel, Interphase Precipitation, Small-Angle-Scattering.

20

21

22

1 High-strength low-alloy steels strengthened through the interphase precipitation (IPP)  
2 mechanism have seen a revival for automotive industry since the development of the  
3 NANOHTEN steel which has tensile strength up to 780 MPa [1]. IPP is the phenomenon  
4 that occurs upon the decomposition of austenite in steels containing strong carbide -forming  
5 elements (such as Ti, Mo and V) and results in characteristic periodic planes of fine  
6 precipitates [2, 3]. In low-carbon steel fine MC (M = Ti, Mo or V) IPP are encapsulated  
7 within a soft ferritic matrix which is strengthened through the Orowan mechanism [4]  
8 yielding a steel with high strength and formability [5].

9  
10 However, these MC particles can coarsen during hot rolling or subsequent annealing heat  
11 treatment, degrading the strength of the materials significantly. One possible solution  
12 reported in the literature is the addition of molybdenum (Mo). Funakawa and Seto [6], and  
13 later work conducted by others [7-10] found that steels with Mo additions showed that the  
14 mechanical properties were retained longer during high-temperature ageing. These studies  
15 were compared to the observed interphase precipitation in Ti-containing (~0.2wt%) and Ti-  
16 Mo-containing (~0.1wt%Ti and ~0.2wt%Mo) low carbon steels with a fixed basic  
17 composition ~0.04%C, 1.5%Mn, 0.2%Si in wt.%. It can be seen that in these studies, the  
18 atomic ratio of Ti:C and (Ti+Mo):C were designed to be ~1:1. The most well-known  
19 mechanism for this effect was reported by Jang et al. [8], who used first principles  
20 calculations to propose that the Mo only participates during the early stages of precipitation  
21 and becomes passive due to the energetic disadvantage during the subsequent growth and  
22 coarsening stages. The coarsening of precipitates is mainly controlled by diffusion of Ti  
23 atoms, therefore, the replacement of Ti by Mo reduces the Ti concentration in the ferrite  
24 matrix, which decelerates the coarsening of (Ti, Mo)C precipitates [6, 8]. Moreover,  
25 Funakawa *et al.* [6] observed that a decrease in Ti concentration from 0.2wt% to ~0.1wt%

1 without Mo additions in Ti-containing steel results in similar hardness of Ti-Mo-containing  
2 one (~0.1wt%Ti and ~0.2wt%Mo). Jang *et al.*, [11] used CALPHAD and diffusion  
3 simulations to show that the coarsening rate of TiC in Fe-Ti-C steels (fixed 0.04%C, wt%)  
4 can be significantly retarded by decreasing the Ti/C ratio.

5

6 However, both the effect of Ti/C ratio and the Mo on the interphase precipitation have not  
7 been well examined quantitatively, which leaves a question to the automotive industry  
8 whether it is necessary to add Mo into Ti-containing steels. This is due to the widely used  
9 techniques such as transmission electron microscopy (TEM) [12, 13] and atom probe  
10 tomography (APT) [14-18] which have a limited capability to analyse statistically significant  
11 numbers of precipitates. The size difference of precipitates in Ti and Ti-Mo steels presented in  
12 the literature is so small (typically in the range of 1.6 nm to 10 nm [7-9]) that it is difficult to  
13 statistically and accurately investigate the the role of Mo with TEM and APT.

14

15 The present study utilizes Small-Angle-Neutron-Scattering (SANS) to study the precipitation  
16 behaviour of two micro-alloyed steels aged at 650°C for various times. One steel (Fe-  
17 0.079Ti-0.051C-1.63Mn-0.19Si-0.036Al-0,014P-0.006S-0.007N, wt%) contains Ti with a  
18 Ti:C atomic ratio of 0.4. The second steel (Fe-0.07Ti-0.2Mo-0.044C-1.58Mn-0.19Si-  
19 0.039Al-0,013P-0.005S-0.0046N, wt%) contains Ti and Mo with a (Ti+Mo):C atomic ratio  
20 of ~1. The detailed characterization was undertaken using SANS, through analysis of both  
21 the nuclear and magnetic signals, giving quantitative insight into the evolution of the average  
22 precipitate size, volume percent, and precipitate chemistry in bulk samples, which are key  
23 information to uncover the precipitation kinetics and hardening behaviour. The data obtained  
24 is averaged over billions of precipitates and provides new insights not available from TEM or  
25 APT where only tens to hundreds of precipitates are typically measured.

1 The alloys were vacuum induction melted, casted and then forged at about 1250 °C followed  
2 by air cooling. Pieces 30×10×5 mm<sup>3</sup> were sectioned and heat treated (See Supplementary Fig.  
3 S1a). Firstly, the specimens were austenitized in a salt bath at 1250 °C for 300 s to dissolve  
4 pre-existing precipitates and water quenched. Secondly, the specimens were austenitized at  
5 950 °C for 120 s (to control the austenite grain size) then transferred directly to a salt bath at  
6 650 °C for periods ranging from 0 to 36 ks and water quenched. Prolonged long-term ageing  
7 for a further 144 ks was performed separately. The austenitization temperature of 950°C and  
8 duration of 120 s were selected in order to balance the compromise between the austenite  
9 grain size, the minimisation of carbide precipitation in austenite. Interphase precipitates can  
10 only form at the advancing austenite/ferrite boundary and therefore, the majority of the Ti, Mo  
11 and C must have remained in solution during austenization. The precipitation-time  
12 temperature diagram obtained by Wang et al. [10] shows that the start times of carbide  
13 precipitation in Ti-Mo (0.1%Ti-0.2Mo%) micro-alloyed steel exceeds 150 s at 950°C.

14

15 SANS experiments were performed on the SANS2d beamline at the ISIS Pulsed Neutron  
16 Source, UK [19]. A magnetic field of 1.5 T was applied to saturate the ferritic matrix which  
17 allows the separation of the magnetic and nuclear scattering. Specimens with dimension of ~9  
18 mm×~9 mm× ~1 mm were cut from the heat treated samples for the SANS measurements.  
19 The neutron beam size was 8mm in diameter and the measurement time was set to 60min.  
20 The sample to detector distance was 4m which gave scattering vector,  $q$ , covered the range of  
21 0.004 to 0.3 Å<sup>-1</sup>. To avoid collecting scattering signal from multi-Bragg diffraction, only  
22 neutrons with wavelengths,  $\lambda$ , from 4.5 to 16.5 Å were selected for data analysis [20]. One-  
23 dimensional nuclear and “nuclear + magnetic” scattering intensity plots,  $I$  (intensity) versus  $q$   
24 were obtained by partial azimuthal averaging in 30 sectors around the horizontal and vertical  
25 axes of the transmitted beam respectively using the software Mantidplot [21].

1 The microstructures of polished and 2% Nital etched samples were examined using scanning  
2 electron microscopy (SEM) via an FEI Quanta 650 FEG-SEM operated at a voltage of 20 kV.  
3 Detailed microstructures of the (Ti,Mo)C precipitates were examined using a JEOL 2100  
4 TEM. Thin foil specimens were mechanically polished to ~30  $\mu\text{m}$  in thickness followed by  
5 ion beam milling to electron transparency. The microhardness (Hv) of ferrite grains in heat  
6 treated samples was measured using a microhardness tester with a load of 0.1 kgf. 20  
7 measurements were conducted for each sample.

8

9 Fig.1a shows the mean value of Hv versus age time at 650 °C for both Ti and Ti-Mo  
10 containing steels and the error-bar represents one standard deviation. The Ti-Mo containing  
11 steels show slightly higher hardness and better ageing-resistance compared to the steel with  
12 only Ti additions. As shown in Figs. 1b and 1c, the  $\gamma$  to  $\alpha$  transformation in both steels occurs  
13 rapidly and both reached ~90% completion in a similar duration of 60 s. This agrees with the  
14 dilatometry results (Supplementary Fig. S1b). Figs. 1b, 1c, 1d and 1e also show that  
15 decreasingly small regions of bainite formed during quenching with increasing isothermal  
16 holding. Both SEM and dilatometry measurements reveal that Mo has a small effect on the  $\gamma$   
17 to  $\alpha$  transformation. Bright field TEM images of the Ti and Ti-Mo containing samples  
18 transformed at 650°C for 36 ks are shown in Figs. 2(e) and (f). In both alloys, characteristic  
19 periodic planes of nanoscale precipitates are observed, indicative of interphase precipitation.

20

21 Fig. 2 shows the one dimensional nuclear and magnetic SANS data in the form of  $Iq^2$  versus  
22 scattering vector ( $q$ ) (left hand axis) for the selected isothermally transformed (60 s, 36 ks  
23 and 180 ks) alloys. The results for the water quenched sample and the remaining isothermally  
24 transformed (0.3ks, 3.6 ks and 18 ks) samples are shown in Supplementary Figs. S2 and S3.  
25 The ratio of magnetic scattering ( $I_{mag}(q)$ ) to nuclear scattering ( $I_{nuc}(q)$ ) intensity,  $R(q)$ ,

1 which is related to the precipitate composition, is shown on the left-hand axis. If all  
2 precipitates have the same composition then the value of  $R(q)$  would be constant. On the  
3 other hand,  $R(q)$  would vary if either there were more than one type of precipitate present of  
4 differing size or the precipitate composition is size dependent [22]. Clearly, there were two  
5 types of particles with significant difference in both size and composition formed in both  
6 steels revealed by two different  $R(q)$  values of  $\sim 3$  and  $\sim 1$  at low ( $0.004$  to  $\sim 0.01 \text{ \AA}^{-1}$ ) and  
7 high ( $0.02$  to  $\sim 0.1 \text{ \AA}^{-1}$ )  $q$  region respectively. A low number density of large ( $> 500 \text{ nm}$ ),  
8 cube-shaped TiN precipitates can be formed during casting process and could remain  
9 undissolved during the experimental solution treatment [10]. These large TiN precipitates  
10 only contribute to the Porod scattering at low  $q$  region  $< 0.001 \text{ \AA}^{-1}$  and has negligible  
11 influence on the scattering signal at  $q$  region  $> 0.01 \text{ \AA}^{-1}$ .

12

13 In the low  $q$  region,  $R(q)$  increases due to the presence of large iron carbides and this is seen  
14 to exist in the Ti-containing steels up to 180 ks. In the Ti-Mo containing steels, there is less  
15 evidence for an increase in  $R(q)$  at low  $q$  suggesting less iron carbide forms in this steel. The  
16 scattering from large scale iron carbides also reveals itself in the form of a Porod Law slope  
17 of approximately  $q^{-2}$  on the plot of  $Iq^2$  versus  $q$  at the low  $q$  region. These large iron  
18 carbides (Figs. 1b and 1c), make only a small contribution to the nuclear scattering signal  
19 (because of their small contrast factor) but a significant contribution to the magnetic  
20 scattering signal. This causes to a marked difference between these two signals at low  $q$  as  
21 revealed by an increase in the  $R(q)$  value. In the samples isothermally held for 180 ks, the  
22 matrix phase transformation was completed so iron carbides did not form following  
23 quenching resulting in a smaller difference between the nuclear and magnetic signals across  
24 the entire range of  $q$ . At high  $q$  region, it is the fine IPP that contribute to the nuclear and  
25 magnetic signals and so  $R(q)$  plateaus from which the chemical composition of the IPP can



1 be estimated. A low number density of large ( $> 500$  nm), cube-shaped TiN precipitates can be  
2 formed during casting process and could remain undissolved during the experimental solution  
3 treatment [1]. These large TiN precipitates only contribute to the Porod scattering at low  $q$   
4 region  $< 0.001 \text{ \AA}^{-1}$  and has negligible influence on the scattering signal at  $q$  region  $> 0.01 \text{ \AA}^{-1}$ .

5

6 To isolate the scattering signal only from nano-sized TiC or (Ti, Mo)C precipitates the Porod  
7 Law region at low  $q$  and the incoherent background in both the nuclear and magnetic SANS  
8 signals were subtracted. Fig. 3 shows the mean values of  $R(q)$ , which were calculated by  
9 taking the average of  $R(q)$  values in the  $q$  range from  $\sim 0.0194$  to  $\sim 0.0775 \text{ \AA}^{-1}$  (for samples  
10 aged for 60s to 3.6 ks) and  $\sim 0.0097$  to  $\sim 0.0664 \text{ \AA}^{-1}$  (for samples aged from 18 ks to 180 ks).  
11 The error in Fig. 3 is given as one standard deviation. The results show that the mean values  
12 of  $R(q)$  for isothermally transformed Ti and Ti-Mo alloys were  $\sim 0.70$  and  $\sim 0.95$  respectively.  
13 The ageing time did not change the mean values of  $R(q)$  significantly. The theoretical  $R(q)$   
14 values of  $\sim 0.64$  and  $\sim 1$  represent the average chemical composition of the precipitates in Ti  
15 and Ti-Mo containing steels are TiC and  $\text{Ti}_{0.75}\text{Mo}_{0.25}\text{C}$  respectively [21], as shown by the red  
16 and blue horizontal lines in Fig. 3. The substitution of Ti with Mo in the precipitates is in  
17 excellent agreement with results obtained from APT [18, 23-24] and extraction [25] in similar  
18 micro-alloyed steels (e.g. 0.05% to 0.2% Ti-0.20%Mo-0.045% C, wt%).

19

20 The volume percent ( $f_v$ ) of TiC and (Ti, Mo)C were calculated from the invariant,  $Q$ , of the  
21 magnetic SANS signal using the equation  $Q = \int_0^\infty I(q)q^2 dq = 2\pi^2 (\rho_p - \rho_m)^2 f_v(1-f_v)$  [21, 26].  
22 where  $\rho_p$  and  $\rho_m$  are the magnetic scattering length densities of precipitate and matrix. The  
23 use of magnetic SANS signal ensures that the volume percent calculation is independent of  
24 the chemical composition of the precipitates. Fig. 4a shows that the volume percent of TiC in  
25 Ti steels and (Ti, Mo)C in TiMo steels were  $\sim 0.10\%$  and  $\sim 0.13\%$  respectively and invariant

1 with isothermal holding. The equilibrium volume percent of 0.156 vol% (TiC phase fraction)  
2 and 0.157 vol% ((Ti, Mo)C phase fraction) at 650 °C calculated using Thermo-Calc and the  
3 TCFE7 database. In the Ti-Mo steel, the equilibrium atomic ratio of Ti to Mo in (Ti, Mo)C  
4 precipitates is predicted to be ~9:1, which indicates the Mo is not strong stabiliser for MC-  
5 type carbide.

6

7 Figs. 4b, 4c and 4d show the Kratky radius ( $R_{max}$ ), Guinier radius ( $R$ ) and thickness ( $T$ )  
8 (disk morphology [24]) of particles obtained from both nuclear and magnetic SANS  
9 scattering signs. The Kratky radius is calculated by  $R_{max} = \sqrt{3}/q_{max}$  (the “pseudo-Guinier  
10 radius”), where the  $q_{max}$  determined from the the Kratky plot ( $Iq^2$  vs  $q$ ) [27]. Alternatively, a  
11 radius of gyration,  $R_{g1}$ , is extracted from the Guinier plot (which takes the form of  $\ln(I)$  vs  $q^2$ )  
12 using a self-consistent method with  $1 < qR_{g1} < 2$ . Considering a distribution of monodisperse  
13 thin discs of thickness,  $T$ , and radius,  $R$ , the relationship between  $T$ ,  $R$  and  $R_{g1}$  is given by  
14  $R_{g1}^2 = T^2/12 + R^2/2$  [28]. A second Guinier plot of  $\ln[q^2(I)]$  vs  $q^2$  is known to give a radius of  
15 gyration,  $R_{g2}$ , that is related to the disc thickness,  $R_{g2} = (T^2/12)^{0.5}$ . Fig. 4b shows that the  
16 average size of the TiC and (Ti, Mo)C interphase precipitates increased from ~6.5nm after  
17 60s to ~10nm after 3.6ks, but exhibit minimal growth during the further ageing up to 180ks at  
18 650°C. The average Guiner radius (Fig. 4c) of disk precipitates has been found ~2nm smaller  
19 than Kratky radius, but followed very similar tendency as kratkey radius. Fig. 4d indicated  
20 that the average Gunier thicknesses of TiC and (Ti,Mo)C were ~5.5nm and ~6.5nm  
21 respectively and both exhibit insignificant evolution (<1.5nm) during isothermal ageing.  
22 Hence, the hypothesis that the Mo can retard the growth and coarsening of (Ti,Mo)C  
23 interphase precipitation is not supported by our results, which show the average precipitate  
24 size in aged Ti-containing steels were even slightly smaller than in aged Ti-Mo-containing  
25 steels.

1  
2 The precipitates coarsening rates in both alloys were extremely low. In Ti-containing steels it  
3 is known that a low Ti/C ratio (0.4) causes the concentration of Ti at the precipitate-ferrite  
4 interface to become small and therefore the diffusion gradients which drive coarsening  
5 become shallow and slow [11]. While in Ti-Mo added steels, although the Ti+Mo/C=1 and  
6 Mo incorporated into the precipitates at nucleation, the subsequent growth of precipitates is  
7 controlled by the diffusion of Ti atoms rather than Mo. We can conclude that the addition of  
8 Mo slightly improved the ageing-resistance of the steels (Fig. 1a) is due to (Ti,Mo)C having a  
9 reduced misfit strain between the carbide and ferrite matrix than TiC [8, 29], rather than Mo  
10 retarding coarsening of the precipitates. Seol et al. [30] and Wang et al. [31-32] indicated that  
11 Mo can segregate at precipitate's outer to form a core-shell structure with Ti-rich core and  
12 Mo-rich shell. Mo layer inhibiting the diffusion of Ti, and V from the matrix into the  
13 precipitates, which impedes particle coarsening. Whether this mechanism exists in Ti-Mo  
14 added steels needs future investigation. The current work only shows the Mo did not retard  
15 the global growth and coarsening of (Ti,Mo)C in 0.07%Ti-0.2%Mo (wt%) micro-alloyed  
16 steels.

17  
18 The addition of Mo also slightly increased the hardness of the steels (Fig. 1a). This is due to  
19 the higher volume percent of interphase precipitates rather than a decreased average size of  
20 precipitate. Approximately 25 at.% Mo co-precipitates as (Mo,Ti)C at the early stage of  
21 precipitation and this increased the volume percent of these precipitates from ~0.1% to  
22 ~0.13%. This yields ~7% improvement in the precipitation strengthening effect based on the  
23 Ashby-Orowan equation  $\Delta\sigma_{ppt} = \frac{0.538Gb f_v^{0.5}}{2R} \ln\left(\frac{R}{b}\right)$  [9, 33, 34]. Where,  $\Delta\sigma_{ppt}$  is the increase in  
24 yield strength,  $G$  is the shear modulus,  $b$  is the Burgers vector,  $f_v$  is the carbide volume  
25 fraction and  $R$  is the mean carbide radius.

1

2 In summary, our SANS results (nuclear and magnetic scattering signals) reveal Mo does not  
3 play a role in retarding nano-precipitate coarsening, which is in contrary to existing literature.  
4 Instead, our results show that approximately 25 at.% Mo replaced Ti in the (Mo,Ti)C  
5 precipitates, increasing both the precipitate volume percent and average size, and changing  
6 the lattice spacing, altering the coherency. Ti-Mo-alloyed steel has higher volume fraction of  
7 nano-precipitates than Ti-alloyed steel hence higher hardness. The better ageing-resistance of  
8 the Ti-Mo steels than Ti only steels is mainly due to the decrease in misfit between the  
9 carbide and matrix leading to coherency being maintained at longer aging times in Ti-Mo  
10 alloyed steel. This new understanding opens opportunities for design of ageing-resistant  
11 micro-alloyed steels with significantly less amount of Mo.

12

### 13 **Acknowledgements**

14 The authors are thankful to Dr Arjan Rijkenberg from Tata Steel for providing the  
15 experimental materials. This work was made possible via funding from the EPSRC (grants  
16 EP/L018705/1, EP/L018632/1, EP/M009688/1 and EP/P012450/1), and the facilities and  
17 support provided by the Research Complex at Harwell. The authors gratefully acknowledge  
18 the use of the SANS2D beamline at ISIS Neutron Source (RB1620206). Dr Wang, Dr Gorley  
19 and Dr Surrey would also like to acknowledge the RCUK Energy Programme under grant  
20 EP/P012450/1 and the UK Government Department for Business, Energy and Industrial  
21 Strategy.

22

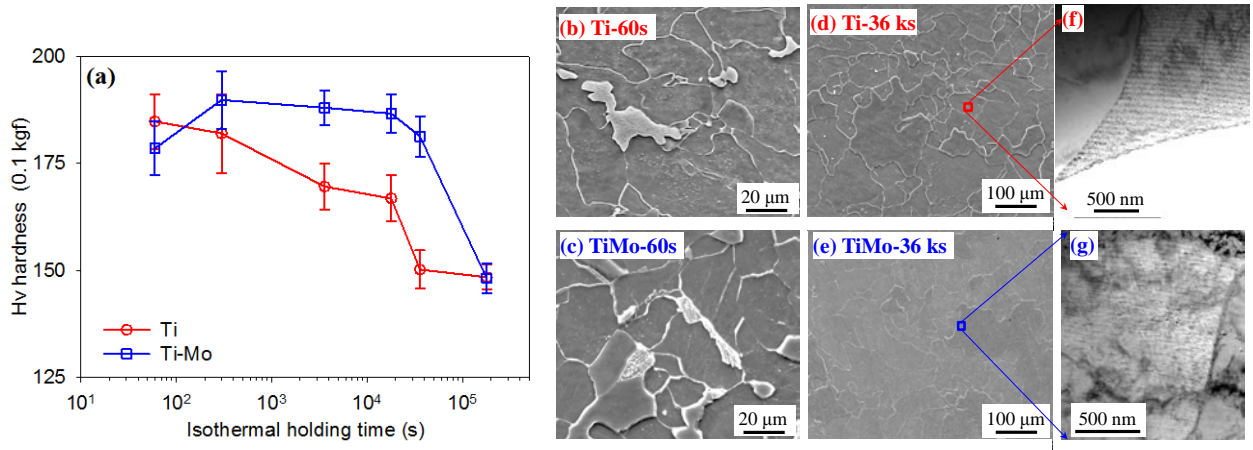
### 23 **References**

- 24 [1] Y. Funakawa, T. Shiozaki, K. Tomita, T. Yamamoto, E. Maeda, *ISIJ Int.* 44(11) (2004)  
25 1945-1951.  
26 [2] A. Davenport, F. Berry, R. Honeycombe, *Metal Sci.* 2(1) (1968) 104-106.  
27 [3] S.-P. Tsai, Y.-T. Tsai, Y.-W. Chen, J.-R. Yang, C.-Y. Chen, Y.-T. Wang, C.-Y. Huang,  
28 *Scr. Mater.* 143 (2018) 103-107.  
29 [4] T. Gladman, *Maney Pub*1997.  
30 [5] F. Yoshimsa, F. Takeshi, Y. Katsumi, *JFE Tech. Rep. No.* 18 (2013).  
31 [6] Y. Funakawa, K. Seto, *Tetsu-to-Hagane.* 93(1) (2007) 49-56.

- 1 [7] C. Chen, H. Yen, F. Kao, W. Li, C. Huang, J. Yang, S. Wang, *Mater. Sci. Eng. A.* 499(1)  
2 (2009) 162-166.
- 3 [8] J.H. Jang, C.-H. Lee, Y.-U. Heo, D.-W. Suh, *Acta Mater.* 60(1) (2012) 208-217.
- 4 [9] N. Kamikawa, Y. Abe, G. Miyamoto, Y. Funakawa, T. Furuhashi, *ISIJ Int.* 54(1) (2014)  
5 212-221.
- 6 [10] Z. Wang, H. Zhang, C. Guo, W. Liu, Z. Yang, X. Sun, Z. Zhang, F. Jiang, *J. Mater. Sci.*  
7 51(10) (2016) 4996-5007.
- 8 [11] J. Jang, C. Lee, H. Han, H. Bhadeshia, D. Suh, *Mater. Sci. Technol.* 29(9) (2013) 1074-  
9 1079.
- 10 [12] H.-W. Yen, P.-Y. Chen, C.-Y. Huang, J.-R. Yang, *Acta Mater.* 59(16) (2011) 6264-6274.
- 11 [13] H.-W. Yen, C.-Y. Huang, J.-R. Yang, *Scripta Mater.* 61(6) (2009) 616-619.
- 12 [14] Y.-J. Zhang, G. Miyamoto, K. Shinbo, T. Furuhashi, *Scr. Mater.* 69(1) (2013) 17-20.
- 13 [15] Y. Kobayashi, J. Takahashi, K. Kawakami, *Scr. Mater.* 67(10) (2012) 854-857.
- 14 [16] I. Timokhina, P. Hodgson, S. Ringer, R. Zheng, E. Pereloma, *Scr. Mater.* 56(7) (2007)  
15 601-604.
- 16 [17] C. Enloe, K. Findley, C.M. Parish, M.K. Miller, B. De Cooman, J. Speer, *Scr. Mater.*  
17 68(1) (2013) 55-58.
- 18 [18] J. Wang, M. Weyland, I. Bikmukhametov, M.K. Miller, P. D. Hodgson, I. Timokhina,  
19 *Scr. Mater.* 160 (2019) 53-57.
- 20 [19] R. Heenan, S. Rogers, D. Turner, A. Terry, J. Treadgold, S. King, *Neutron News* 22(2)  
21 (2011) 19-21.
- 22 [20] A. Michels, J. Weissmüller, *Rep. Prog. Phys.* 71(6) (2008) 066501.
- 23 [21] Y. Wang, S. Clark, V. Janik, R. Heenan, D.A. Venero, K. Yan, D. McCartney, S. Sridhar,  
24 P. Lee, *Acta Mater.* 145 (2018) 84-96.
- 25 [22] B.S. Seong, E. Shin, S.-H. Choi, Y. Choi, Y.S. Han, K.H. Lee, Y. Tomota, *Appl. Phys.*  
26 *A* 99(3) (2010) 613-620.
- 27 [23] I. Bikmukhametov, H. Beladi, J. Wang, P. D. Hodgson, and I. Timokhina, *Acta Mater.*  
28 170 (2019) 75-86.
- 29 [24] S. Mukherjee, I. Timokhina, C. Zhu, S. Ringer, P. Hodgson, *Acta mater.* 61(7) (2013)  
30 2521-2530.
- 31 [25] Y. Tanaka, S. Kinoshiro, H. Nakamichi, *JFE Tech. Rep. No.* 37 (2016) 31-36.
- 32 [26] F. De Geuser, A. Deschamps, *C R Phys* 13(3) (2012) 246-256.
- 33 [27] A. Deschamps, F. De Geuser, *J. Appl. Crystallogr.* 44(2) (2011) 343-352.
- 34 [28] H. Yasuhara, K. Sato, Y. Toji, M. Ohnuma, J. SUZUKI, Y. Tomota, *Tetsu-to-Hagane.*  
35 96(9) (2010) 545-549.
- 36 [29] J. Jang, Y. Heo, C. Lee, H. Bhadeshia, D.-W. Suh, *Mater. Sci. Technol.* 29(3) (2013)  
37 309-313.
- 38 [30] Z. Wang, H. Chen, Z. Yang, F. Jiang, *Metall. Mater. Trans. A* 49, no. 5 (2018): 1455-  
39 1459.
- 40 [31] Z. Wang, X. Sun, Z. Yang, Q. Yong, C. Zhang, Z. Li, Y. Weng, *Mater. Sci. Eng. A.* 573  
41 (2013): 84-91.
- 42 [32] J. B. Seol, S. H. Na, B. Gault, J. E. Kim, J. C. Han, C. G. Park, D. Rabbe, *Sci. Rep.* 7  
43 (2017) 42547.
- 44 [33] M.-Y. Chen, M. Gouné, M. Verdier, Y. Bréchet, J.-R. Yang, *Acta Mater.* 64 (2014) 78-  
45 92.
- 46 [34] P. Gong, X. Liu, A. Rijkenberg, W. Rainforth, *Acta Mater.* 161 (2018) 374-387.

47  
48  
49  
50

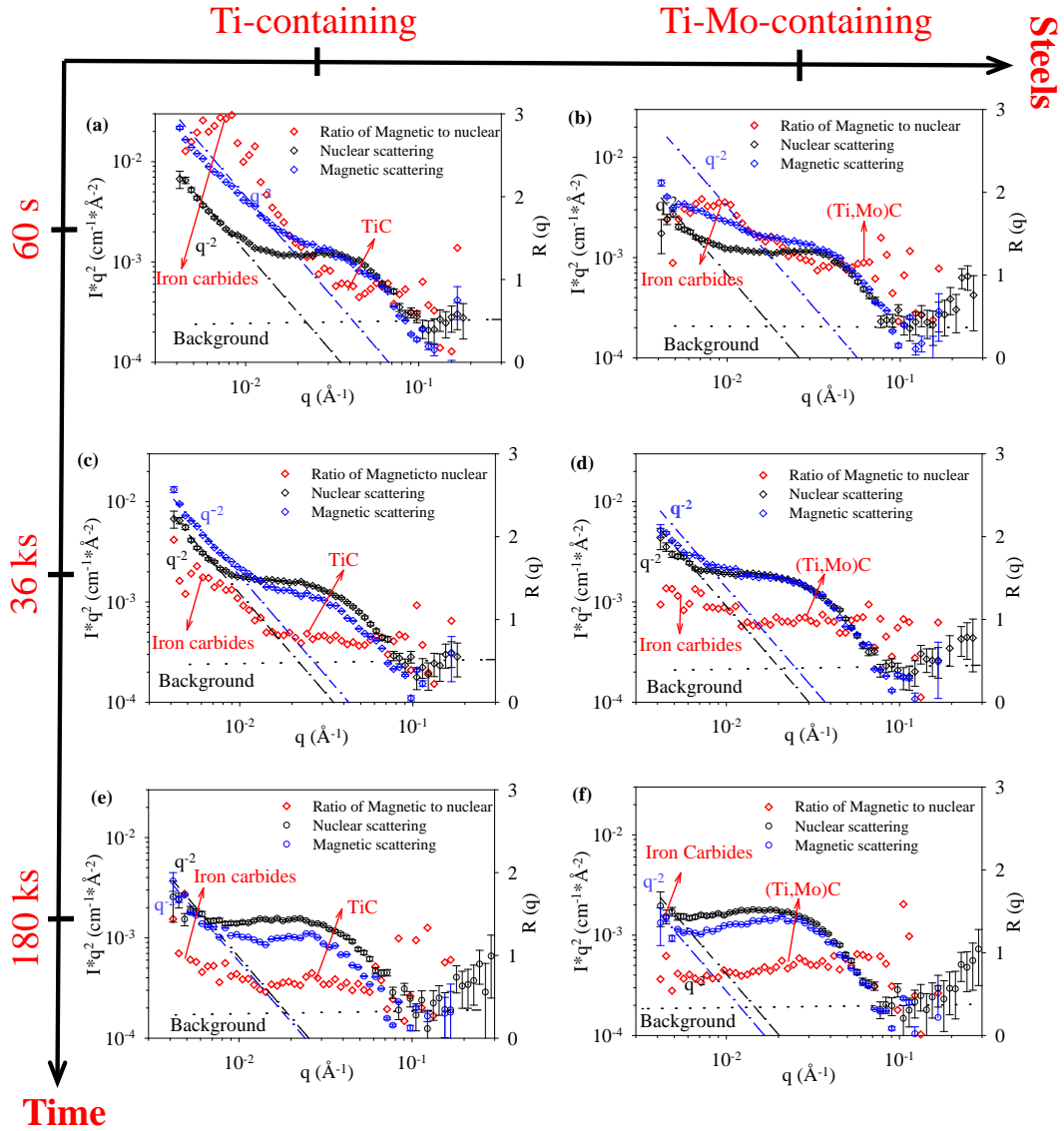
1  
2  
3  
4  
5



6

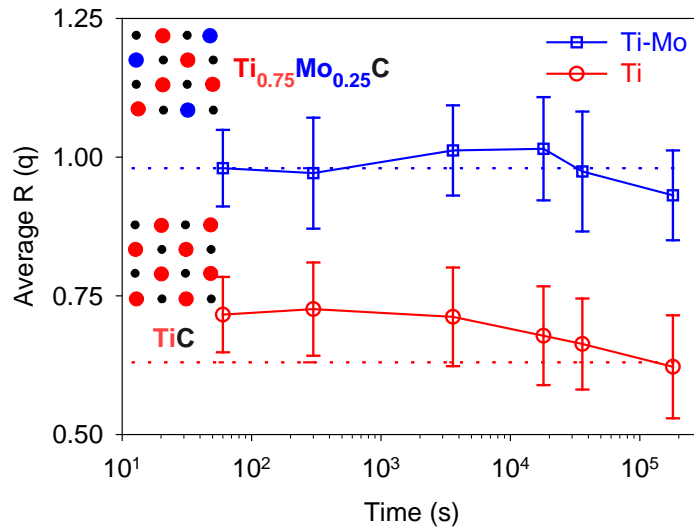
7 Fig. 1. (a) Effect of isothermal holding time,  $t$ , on measured microhardness,  $H_v$ , of the Ti and  
8 Ti-Mo steels held at 650 °C. Error bars in  $H_v$  correspond to one standard deviation from the  
9 mean. (b) to (e) SEM images of the Ti (b and c) and TiMo (d and e) samples isothermally  
10 transformed for 60 s and 36 ks. (f) and (g) Bright field TEM images of the Ti and TiMo steels  
11 respectively after ageing for 36 ks showing interphase precipitation.

12  
13



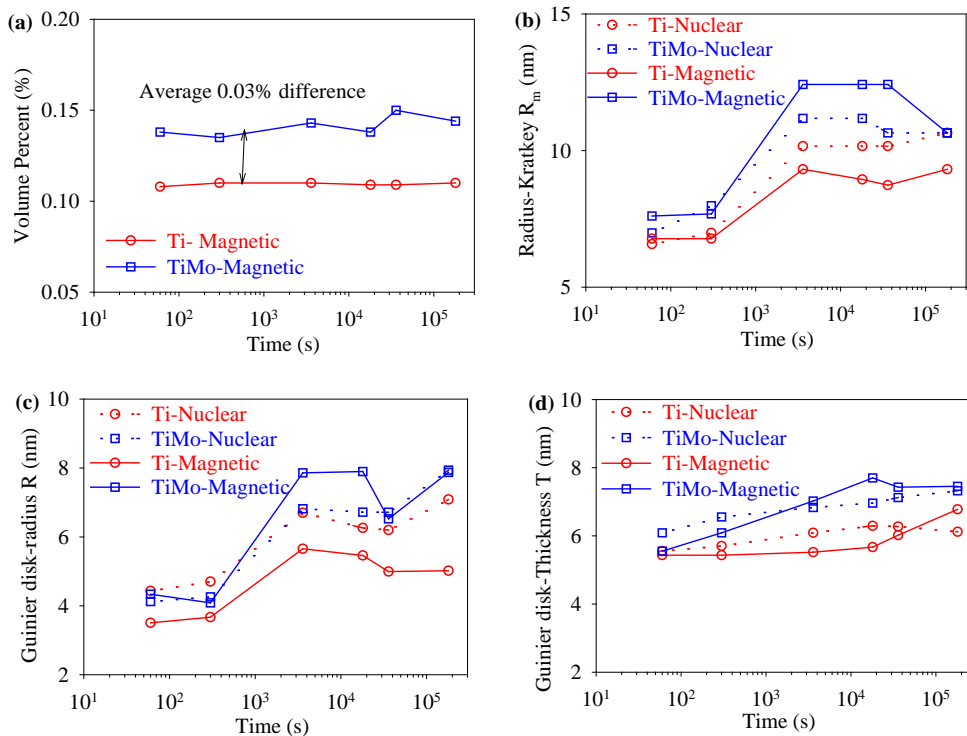
1

2 Fig. 2. One-dimensional nuclear and magnetic SANS patterns of  $Iq^2$  (left hand axis) and  $R(q)$   
 3 (right hand) axis versus scattering vector,  $q$ , obtained from the (a, c and e) Ti and (b, d, and f)  
 4 TiMo samples isothermally transformed at 650 °C for (a and b) 60 s, (c and f) 36 ks, (e and f)  
 5 180 ks respectively.  
 6



1  
2  
3  
4  
5

Fig. 3. Plot of the mean value of  $R(q)$  as a function of scattering vector,  $q$ , calculated from the scattering curves in Fig. 2.  $R(q)$  is the ratio of magnetic to nuclear scattering intensity. Theoretical values for TiC and for  $Ti_{0.75}Mo_{0.25}C$  are shown by the horizontal lines.



6  
7  
8  
9  
10  
11  
12  
13  
14

Fig. 4. Graphs to show the effect of isothermal holding time,  $t$  on carbide particle volume fraction and particle dimensions in Ti and TiMo alloys aged at 650 °C. (a) Particle volume percent calculated from analysis of the invariant,  $Q$ , of the magnetic SANS data. Particle dimensions obtained from (b) Kratky radius,  $R_{max}$ , assuming spherical-shaped particles and (c and d) Guinier analysis assuming disk-shaped particles. (c) shows the disk radius,  $R$ , versus ageing time,  $t$ , and (d) shows disk thickness,  $T$ , versus time,  $t$ .